

ON THE BIOLOGICAL SHAPE OF THE POLYGONACEAE RHEUM PETIOLE

D. PASINI

Department of Mechanical Engineering, McGill University, Montreal, Canada.

ABSTRACT

The petiole is a plant organ that connects the stem to the blade of a leaf. The petiole is made up of a fibrous biomaterial that consists of three integrated tissues. Each of these specializes in different functions, but they work together to provide basic needs, such as nutrient transport, food storage and plant support. From a structural viewpoint, the petiole resembles a cantilever that should resist wind torsion and gravity bending forces acting on the leaf blade. It has a solid cross-section with a grooved flattened asymmetric shape with size decreasing lengthwise. As all plant organs, the petiole morphology is developed by adaptive growth, which is the plant response to environmental stimuli. Thus, the petiole grows a shape that best optimizes the use of vital resources. This paper focuses on the structural efficiency of the shape petiole and it examines the capability of the petiole in reducing the wind drag without sagging under gravity forces. Continuum mechanics and dimensionless factors are used to model the twist-to-bend ratio. Twenty specimens of Polygonaceae *Rheum rhabarbarum* plants were investigated. The results are visualized on maps that contrast the petiole shape properties to those of ideal cross-sections.

Keywords: bending stiffness, leaf petiole, optimized shape, structural efficiency, torsional compliance, twist-to-bend ratio.

1 INTRODUCTION

During growth, a plant develops roots, stems, branches and leaves. These organs work in synergy to satisfy the basic needs for survival, such as support, transport and storage of food. The leaf is the crucial organ for photosynthesis. It allows the plant to process the sun's energy and produce sugar for its own life [1].

From a structural point of view, the leaf has a noteworthy structure consisting of a blade upheld by a stalk, or petiole. The morphology of the petiole is designed to minimize the use of resources for load support. In the absence of wind, for example, the petiole resembles a cantilever beam that is equipped with sufficient resistance to keep the blade from being exposed to the sun without collapsing under gravity loads. In the moving wind, on the other hand, the petiole functions as a bar, where the aerodynamic forces acting on the frontal area of the blade exert twisting actions. Against these, the petiole offers little resistance to ease the cluster of the leaves and reduce the area of the leaf exposed to wind. As a result, the wind drag on the leaf is dropped and the material required to withstand external forces is reduced.

The capabilities to keep the blade exposure from sunlight, as well as to allow leaf reconfiguration in high wind, are governed by the biomechanical properties of the petiole [2–6]. The material and the geometric properties of the petiole play a crucial role in the flexural stiffness and in the torsional flexibility. The former describes the bending resistance against gravity forces, whereas the latter governs the petiole compliance to wind action. Their ratio is the twist-to-bend index that has been used to examine the ability of living organisms to twist without bend [2–14].

Simplified models and testing apparatus have been proposed to predict and measure respectively the elastic and viscoelastic properties of stems for different plant species [2–19]. Plotting the bending stiffness against the torsional rigidity eases the visual characterization of the specimen properties. More recently, graphical approaches have also been adopted to contrast biological beams to engineering beams of ideal shapes [14, 20]. Such a visual comparison of nature to engineering

design has been suggested to be conducive to capture novel material and geometry design. This rationale applies also to this work that aims at gaining insight into why the shape of the Polygonaceae *Rheum rhabarbarum* petiole grows as they do.

This study examines the structural efficiency of the petiole cross-section at the internode with the stem. The focus is placed on the relationship between the morphological design of the leaf petiole and its structural performance in carrying multiple loading. This paper starts off with an overview of the plant functions and a general description of the factors that trigger morphological changes. Then the zoom is onto the petiole organ, especially on its structural mechanics. A scheme for characterizing the structural contribution of the petiole cross-sections is presented in terms of shape parameters. These have been introduced to model shape performance at different length scales for alternative shape cross-sections [21–24]. In this work, the method is extended by using the concept of *superellipse* [25–29] to describe natural shapes [30–33]. Lamé curves are used to fit the profiles of a range of asymmetric shapes and to formulate shape transformers for the twist-to-bend ratio. These concepts are then contrasted to the *Rheum rhabarbarum* specimen and visualized on performance maps to gain insight into the shape efficiency of the petiole cross-sections.

2 PLANT ORGANS AND FUNCTIONS

Angiosperms are flowering plants whose reproductive organs are within flowers, and seeds (i.e., cotyledons) are in the fruits. The number of seeds is used to sort angiosperms into two classes: the monocots, which have a single cotyledon, and the dicots with two seeds. The *Rheum rhabarbarum* falls into the latter.

Monocots and dicots have morphological differences. Unlike dicots, monocots have parallel veins in the leaf, a fibrous root system and vascular bundles complexly arranged. Dicots, on the other hand, present netlike leaf veins, a taproot system, which consists of a major root growing vertically, vascular bundles usually arranged in a ring and floral parts in multiples of four or five [1].

Despite the differences, there are also features common to all angiosperms: the root and the shoot system. The main vital functions of roots are the absorption of water and minerals, their conduction from the roots to the stem and vice versa, and lastly, the storage of food. The structural function of the roots is to provide anchor in the soil. On the other hand, the shoot system consists of the stem, which supports the leaves and the photosynthetic organs (Fig. 1).

3 TRIGGERS FOR MORPHOLOGICAL CHANGES

Like most living organisms [2, 34, 35], a plant is a complex system with highly integrated organs and tissues. Each of these has multiple vital functions that are optimized to meet basic vital needs, such as mineral absorption, water supply, photosynthesis, food storage and structural support.

The morphology of plants is governed by a process of adaptive growth. As they grow, plant organs shape their bodies in response to environmental stimuli. They can detect changes of light, loading, soil salinity and stress concentration and, in response, they adapt their morphology at the macro as well as micro level. Some changes are governed by reversible movements and are described in Section 3.1. Others that usually impose permanent traits are reported in Section 3.2.

3.1 Morphological changes due to tropisms and turgor movements

Tropism is a response of the plant curvature to stimuli. If the plant curves toward the stimuli, the tropism is positive, whereas it is negative when the plant curves away from it. The turgor movements are usually rapid and reversible, often due to pressure changes within the cells subject to stimuli.

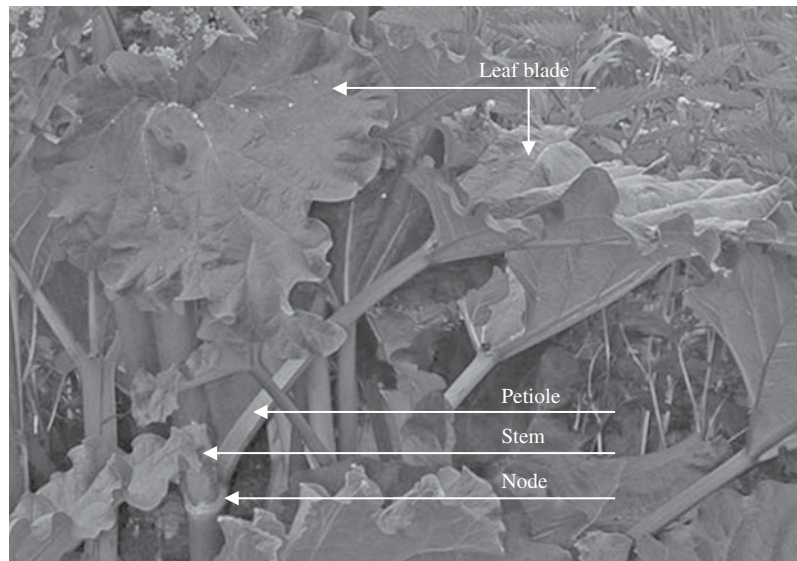


Figure 1: The triangular blade and the grooved stalk of a Polygonaceae *Rheum rhabarbarum* plant. (Adapted image by Jan De Laet, © 2006.)

For example, *phototropism* is the bending of a plant either towards or away from a light source and it allows photosynthesis to take place. *Sleep movements* are also responses to changes of light during the course of the day. Legumes and bean plants, for instance, raise their leaves horizontally in the morning, and lower them vertically at sunset. *Gravitropism*, on the other hand, is the plant response to gravity. When it is positive, the roots grow deep into the soil to secure water and other nutrients. If it is negative, the shoots develop up towards the sunlight. *Thigmotropism* is a directional growth in reaction to touch. Unlike stems that grow straight, vines, for example, have tendrils that coil at touch with an object.

3.2 Morphological changes in response to environmental stresses

Variations in temperature, stress and water content are factors that induce morphological adaptations at different length scale, from the cellular to the meso-scale. These may have a strong impact on the plant morphogenesis.

Oxygen deprivation and *cold temperature* are examples of such triggers. As a result of the former, the growth of air tube cells in certain roots is accelerated to allow oxygen supply. Due to the latter, the plant is called to increase its amount of unsaturated fatty acids. *Excess of sodium* also threatens plant growth. Salt can cause the root to lose water, even when the soil is submerged in water. This phenomenon occurs when the osmotic pressure of the surrounding water is not as high as that of the root tissue. Another trigger is the *water deficit* that stimulates the synthesis of a hormone (i.e., abscisic acid). This substance induces the pore closure and reduces evaporation. Cells lose turgidity and expose less surface to the sun. As a result, when the level of environmental factors, such as water retention and insulation, is severe, shape adaptation occurs at the tissue level as well as at the macro-level of each plant organ.

Another factor causing modifications of the micro and macroscopic structure is the *critical stress regime* induced by physical forces. The plant builds tissues under adaptive growth, mainly by responding to compressive stresses [36–38]. This phenomenon that starts at the cellular level is crucial in determining the morphology of a plant organ. Within the tissues, fibers grow aligned to the orientation of the internal forces and in regions of critical compressive stresses. The additional fibers work like reinforcements that lower the stress regime below the compressive strength to prevent the buckling failure of cell walls.

4 THE PROFILE OF THE POLYGONACEAE *RHEUM RHABARBARUM*

The *rhabarbarum* species falls into the *Rheum* genus of the *Polygonaceae* family of dicotyledons. It is a perennial plant often cultivated in Europe and North America, in Western and North-western provinces of China, and in Tibet. The *Rheum rhabarbarum* grows from short rhizomes, forms thick and long stalks, and develops large leaves, as shown in Fig. 1. Its flowers are small, greenish-white, and borne in large compound leafy inflorescences.

The typical size of rhubarbs varies from 3 to 5 feet height, or even more, with 3–4 feet width. The structure of a leaf resembles a flat blade, which is connected to the stem by a petiole at an angle with the horizontal. The blade has a large size with width and length that grow up to 1 foot or more. Its form is roughly triangular (Fig. 1). The blade is the part of the leaf that is poisonous because it contains high concentrations of inedible oxalic acid crystals. The petiole is fleshy and slender with a length of up to 18 inches long and 1–2 inches in diameter. The cross-section is solid with roughly semi-elliptical shape, as shown in Fig. 2.

Cross-sections with similar semielliptical shapes can be found in different petioles that twist easily before sagging under gravity load. For example, top groove and U-shapes are distinctive of banana and green bean plants [6]. These geometries, however, are not the only one found in plants. Elliptical shapes, for instance, are quite common in horizontal branches of trees. Here, an important factor determining specific morphology adaptations is the scaling effect. During growth, cross-sections evolve with respect to the scaling rule of the acting forces. In horizontal branches, the own weight increases with the size cubed and is dominant at large scale, whereas the wind loading is governed by the size square. Thus, it is not surprising small branches exhibit circular cross-sections. On the other hand, large-scale branches grow superelliptical shapes, which are often elongated along the downward direction to maximize the resistance to bending stresses [6, 12, 13]. Besides environmental factors, magnitude and direction of loads, as well as scaling effects, another factor to consider is the joint between the stem and the petiole. As the petiole grows from the stem,

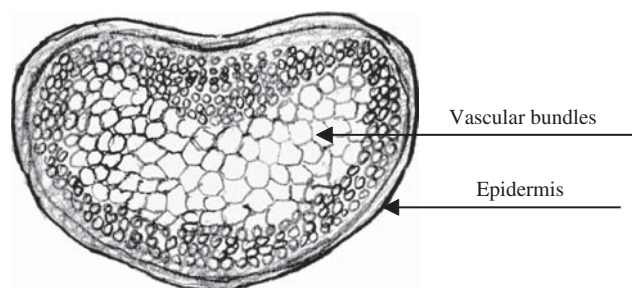


Figure 2: Sketch of a rhubarb petiole cross-section.

the size of the latter constrains the maximum size that the petiole cross-section can develop along its width [12].

4.1 The histology of the bio-material

In contrast to homogeneous, elastic and isotropic materials, the rhubarb is made up of a composite microstructured material, whose anisotropy is governed by three living tissues. Each of these is made of similar cells clustered into units that grow continuously throughout the plant. Each cell has a cellulose wall that contains a large sap filled vacuole.

To better understand the anatomy of the tissues, botanists group plant tissues into three main systems: the dermal, the vascular, and the ground system. As described below, each of them performs multiple vital functions, but not all of them provide structural support.

4.1.1 Vital functions of the tissues

- *The dermal system* is the outer epidermis and is analogous to our skin (Fig. 2). It consists of a layer of tightly packed cells that protect plant organs. The cells line internal cavities and exposed surfaces. The dermal tissue, covered by a waxy coating, called cuticle, has the function of reducing water loss through evaporation. The pores, stomata, control the exchange of gases between the plant and its surroundings. Thus, the cuticle is a crucial protection, especially in dry summers.
- *The vascular system* consists of vascular bundles grouped into two tissues: the Xylem and the phloem (Fig. 2). The former conveys water and minerals from roots into the shoots. The latter is in charge of transporting food from mature leaves to the roots, as well as to parts of the shoot system (e.g., developing leaves and fruits).
- *The ground system* is the parenchyma that governs the metabolic processes, beyond photosynthesis and food storage. Its cells are mainly made up of thin walled cells with large vacuoles.

4.1.2 Structural functions of the tissues

The parenchyma and the vascular bundles make up the bulk of the plant and are the tissues providing support. The former has cellulose cells and fills the space between the dermal and the vascular systems. When soaked with water, the cells are turgid, and this turgor allows the plant to keep upright. The latter, in particular the xylem tissue, has structural reinforcements along the Tracheary vessels. These fibers are shaped in thick hollow tubes that provide higher stiffness and strength compared to a solid cylinder of the same mass. Reinforcement is obtained by constraining the vessels with spiral hoops of lignin arranged at a certain angle with the tube axis. The coils work as reinforcing belts that impede the radial deformation induced by water pressure on the tube walls.

In the shooting system, there are other structural tissues beyond parenchyma and vascular bundles. One is the collenchyma, which has thick, relatively flexible cell walls, which are rich in pectic substances. Pectic confers ductility to the stalks and allows it to deform without failure. The other is the sclerenchyma that provides cells the elasticity, which allows the petiole to return to its original configuration upon deformation.

5 THE STRUCTURAL FUNCTIONS OF THE PETIOLE

From a structural point of view, the petiole of the rhubarb (Fig. 1) resembles a cantilever beam subjected to bending and torsion. The former is induced by gravity loads, such as the blade weight, as well as other loads, like rain, snow, moisture, or the weight of an insect. The latter results from twisting triggered either by the aerodynamic wind action on the blade or by phototropism.

The petiole morphological design is different than that of the stem. The structure is tapered lengthwise and has an asymmetric flattened cross-section, often grooved at its top. Its mechanical properties are governed by factors involving its material and geometry. However, in contrast to engineering technology, nature does not make a clear distinction between them. The biomaterial is not homogeneous and its structural response is determined by several factors including cell's material, the arrangement of the tissues, the way in which the fibers are assembled, and the degree of interaction between them. The analysis of this paper examines the role of the geometry. A more comprehensive model that takes into account material anisotropy is left to future work.

The model is based on classic mechanics, although limitations exist for its application to the biological world. The material is assumed to be isotropic and homogeneous, and the geometry is assumed to satisfy Euler–Bernoulli beam theory. Shear deformations are not considered. The ideal case is a slender element of length L with Young's modulus E and shear modulus G . The beam carries a uniform torsion T and bending M at one end and their corresponding equilibrium moments at the other free end. The bending and torsion stiffness for a cantilever beam of length L are respectively:

$$k_b = \frac{EI}{2L^2} \quad (1)$$

$$k_t = \frac{GJ_T}{L} \quad (2)$$

where I and J_T are the second moment of area and a torsional constant depending on the cross-sectional shape. J_T is the polar moment for circular shape shafts that do not experience warping; for non-cylindrical bars, whose cross-sectional planes do not remain plane after twisting, J_T is a function of warping [39, 40].

Flexibility is a recurrent feature in plants enabling the impact of the loading and of the induced stress regime to be reduced. For the petiole, torsional compliancy is more important than flexural flexibility. A high torsional flexibility is beneficial because it can reduce the wind-drag up to 30%, as in the case of daffodils [3, 5]. Banana leaves and sedges are also easy to twist which allow them to swing around in wind rather than bending over [11, 12]. To measure the resistance to bending relative to twisting, we resort to the twist-to-bend ratio k_b/k_t , which from (1) and (2) is given by:

$$\frac{k_b}{k_t} = \frac{1}{2L} \frac{EI}{GJ_T} \quad (3)$$

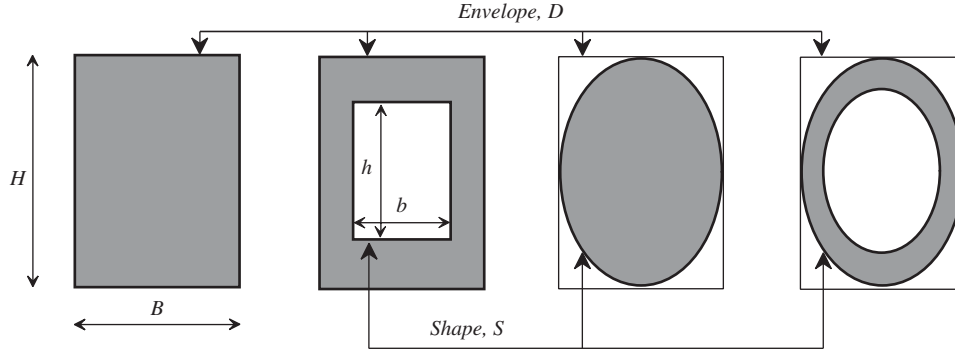
For a given length, the geometry in (3) is described by I/J_T and it is strongly dependent on the shape and size of a cross-section. The following section describes a scheme to characterize the shape properties of a cross-section for given structural requirements.

6 MODELING THE TWIST-TO-BEND RATIO OF THE PETIOLE

A method has been recently introduced to gain insight into the shape performance of engineering structures [21–23]. This scheme is reviewed in Section 6.1; it is extended in Section 6.2 and applied in Section 6.3 to the petiole analysis.

6.1 The methodology

The scheme is based on the idea that the geometry of a cross-section can be described by two distinct contributions. The first is related to the size of the cross-section, the second to its shape. The size is

Figure 3: Shape, S , and envelope, D , of different cross-sections.

described by a rectangle with the main dimensions of the cross-section and it is referred to as the envelope D , as shown in Fig. 3. S represents the shape of the figure enclosed in D and its properties are dimensionless.

The idea of decoupling D from S leads to the definition of scalar operators that deal with the scaling and the shaping of a cross-section. The former is described by the envelope multipliers, u and v , and the latter by the shape transformer ψ_g .

Envelope multipliers. If B_o and H_o are the width and height of a reference rectangle, the scaling relations of a generic envelope (B, H) relative to the reference are respectively $u = B/B_o = b/B$ and $v = H/H_o = h/H$, where b and h are the internal dimensions of a hollow cross-section (Table 1a).

Shape properties. The shape transformers are formulated by normalizing a geometric quantity, g , of a cross-section with the same geometric quantity, g_D , of its envelope such that:

$$\psi_g = \frac{g}{g_D} \quad (4)$$

For example, area, second moment of area about the x axis, and the torsional constant are geometric quantities that can be respectively expressed through relation (4) in terms of shape properties as:

$$\left\{ \begin{array}{l} \psi_A = \frac{A}{A_D} \\ \psi_{I_{xx}} = \frac{I_{xx}}{I_D} \\ \psi_{J_T} = \frac{J_T}{J_{TD}} \end{array} \right. \quad (5)$$

J_T for circular shapes is exactly the polar moment of area J . For other shapes, this is not the case and replacing J_T with J may involve an approximation of up to 15% [24]. In this work, the torsional constant J_T is simplified to the polar moment of area.

As shown in Fig. 2, the cross-section of the petiole rhubarb possesses one axis of symmetry. Table 1a summarizes the shape transformer expressions for three shapes that have a vertical axis of symmetry and that may evolve in shape with double symmetry. Here, we consider shapes that have

Table 1a: Shape transformers for shape families.

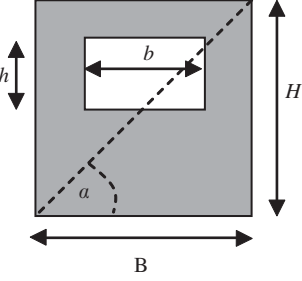
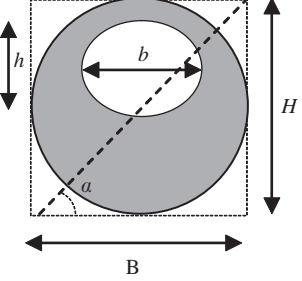
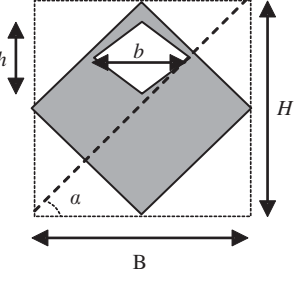
The rectangle family	The ellipse family	The diamond family
		
	$\psi_A = \beta_1 [1 - cd]$	
$\beta_1 = 1$	$\beta_1 = \frac{\pi}{4}$	$\beta_1 = \frac{1}{2}$
$0 \leq \psi_A \leq 1$	$0 \leq \psi_A \leq \frac{\pi}{4}$	$0 \leq \psi_A \leq \frac{1}{2}$
	$\psi_{Ixx} = \beta_2 \left[1 - cd^3 - PA \right]$	
$\beta_2 = 1$	$\beta_2 = \frac{3\pi}{16}$	$\beta_2 = \frac{1}{4}$
$0 \leq \psi_{Ixx} \leq 1$	$0 \leq \psi_{Ixx} \leq \frac{3\pi}{16}$	$0 \leq \psi_{Ixx} \leq \frac{1}{4}$
	$PA = \beta_3 \left[cd \left(\frac{1 - cd(2d_1 + d)}{2(1 - cd)} - d_1 - \frac{d}{2} \right)^2 \right]$	
$\beta_3 = 12$	$\beta_3 = \frac{3}{4}$	$\beta_3 = \frac{1}{2}$
	$\psi_J = \beta_5 \left[1 - cd^3 + \cos^2 \alpha (cd^3 - c^3 d) \right]$	
$\beta_5 = 1$	$\beta_5 = \frac{3\pi}{16}$	$\beta_5 = \frac{1}{4}$
$\alpha = 0, 90 : 0 \leq \psi_J \leq 1$	$\alpha = 0, 90 : 0 \leq \psi_J \leq \frac{3\pi}{16}$	$\alpha = 0, 90 : 0 \leq \psi_J \leq \frac{1}{4}$

Table 1a: (Continued)

The rectangle family	The ellipse family	The diamond family
$\lambda_I = \beta_4 \left[(1 - cd^3 - PA)(1 - cd)^{-1} \right]$		
$\beta_4 = 1$	$\beta_4 = \frac{3}{4}$	$\beta_4 = \frac{1}{2}$
$1 \leq \lambda_I \leq 3$	$\frac{3}{4} \leq \lambda_I \leq \frac{9}{4}$	$\frac{1}{2} \leq \lambda_I \leq \frac{3}{2}$
$\lambda_J = \beta_6 \left[\frac{1 - cd^3 + \cos^2 a (cd^3 - c^3 d)}{1 - cd} \right]$		
$\beta_6 = 1$	$\beta_6 = \frac{3}{4}$	$\beta_6 = \frac{1}{2}$
$a = 0, 90 : 1 \leq \lambda_J \leq 2$	$a = 0, 90 : \frac{3}{4} \leq \lambda_J \leq \frac{3}{2}$	$a = 0, 90 : \frac{1}{2} \leq \lambda_J \leq 1$
$\frac{\psi_I}{\psi_J} = \left[\frac{1 - cd^3 - PA}{1 - cd^3 + \cos^2 a (cd^3 - c^3 d)} \right]$		
$a = 0, 90 : \frac{\psi_I}{\psi_J} = 1$	$a = 0, 90 : \frac{\psi_I}{\psi_J} = 1$	$a = 0, 90 : \frac{\psi_I}{\psi_J} = 1$

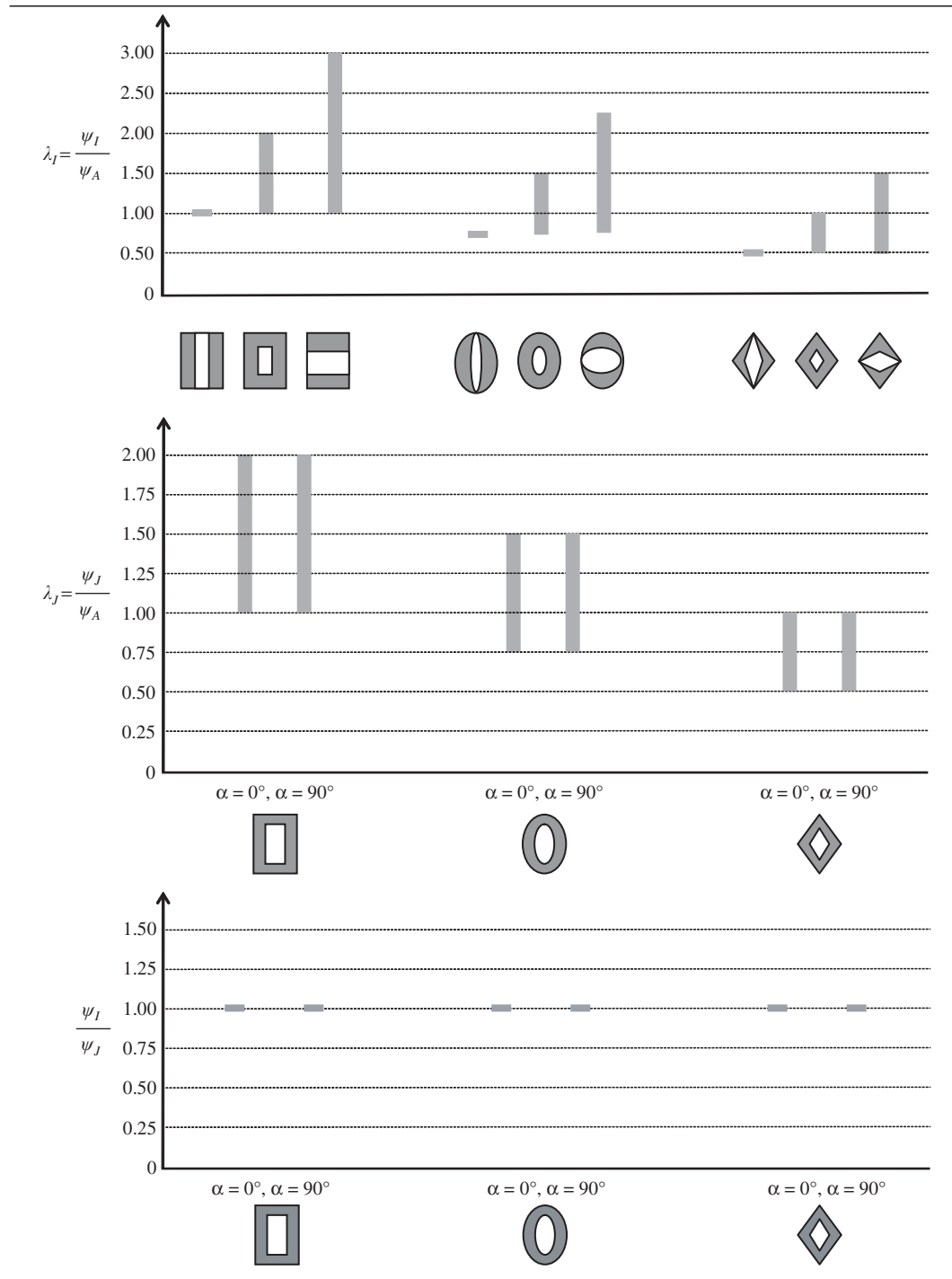
at least one axis of symmetry to avoid asymmetric bending. ψ_A , ψ_{Ixx} and ψ_J have values that vary with respect to the area filling the envelope. When the material saturates the shape completely, ψ_g for the resulting solid shape assumes an upper bound of the range, as shown in Table 1a and b; whereas for hollow shapes, it may decrease to zero, which corresponds to an empty shape.

The underlying principle of the shape transformers is that the scheme allows the decoupling of S from D . When an equation of mechanics is expressed by a product $F \times M \times g$, where F describes the problem specifications, M the material properties, and g an aspect of the geometry, then applying (5) enables its reformulation in terms of four factors as $F \times M \times \psi_g \times g_D$. The advantages of this rationale have been illustrated in material and shape selection [21–23]. In the next section, shape transformers are formulated for super-elliptical shapes and are then applied to the structural analysis of the petiole in Section 6.3.

6.2 A shape classification

Shape transformers have been used to define families and classes of shapes, in a way similar to material classification [22]. Here, we use the Lamé curves to define families of shapes and to formulate the shape transformers. Lamé curves, also known as super-ellipses, have been used as a design tool for a variety of applications ranging from engineering to architecture and urban design [41].

Table 1b: Range of shape transformers for shape classes.



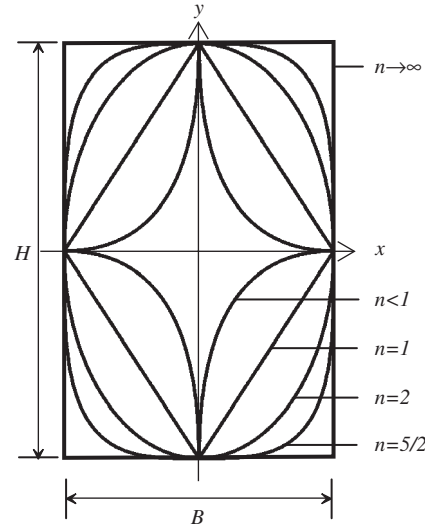


Figure 4: Superellipses within the envelope $B \times H$. n governs the shape profiles.

Lamé curves were named in 1818 by the French mathematician Gabriel Lamé (1795–1870) [25–32]. In their implicit form, these curves are given by

$$\left| \frac{x}{a} \right|^n + \left| \frac{y}{b} \right|^n = 1 \quad (6)$$

where n can be any rational number, and a and b are positive real numbers describing the radii of the oval shape.

As shown in Fig. 4, Lamé curves are smooth curves whose profile is determined by the exponent n . Nine types of Lamé curves can be defined with respect to the value of the exponent n . Two categories are defined for: $n > 0$, $n < 0$. Here, we resort to the subset of Lamé curves, where n is a positive integer. The case $n = 2$ yields an ordinary ellipse. As n increases beyond 2, the curve becomes a superellipse, flatter and flatter at the intersection with the x and y axes; it is a rectangle for $n \rightarrow \infty$. A decrease of n below 2 yields hypoellipses, which increasingly resemble crosses with sharp corners at the x and y axes.

Table 1 illustrates three shape families that are obtained for $n = 1$, $n = 2$, and $n \rightarrow \infty$, with $a = B/2$ and $b = H/2$. Each of these describes a shape concept and represents a family. Within a family, there are solid and hollow cross-sections independent of their size. Hollow shapes fall into a family if both the internal holes and external contours have the same exponent n of the Lamé curves. The classification of family members into classes is determined by the scaling relation between the internal hole and the envelope. Three scaling modes applied to the internal contour are considered here: vertical ($c = 1$), proportional ($c = d$), and horizontal ($d = 1$).

Similar to materials, shapes of a family exhibit properties that fall into a particular range, as shown in Table 1b. For example, the ratio $\lambda_I = \psi_I/\psi_A$ measures the lightweight efficiency of a uniform and isotropic material distribution in design for bending stiffness. The higher the value of λ_I , the stiffer to bending as well lighter is the shape. The ratio $\lambda_J = \psi_I/\psi_A$ is another measure of the

lightweight potential of a shape in torsional stiffness design (Table 1a and b). Table 1b shows that each class is governed by a specific range of λ_I and λ_J . Although these ranges are theoretical, since they do not account for manufacturing constraints, shear and buckling failure requirements, they are helpful to compare shape concepts for preliminary shape optimization.

6.3 Shape transformers applied to the twist-to-bend ratio

To assess the impact of the shape transformers on the twist-to-bend ratio of a unit length petiole, we substitute ψ_I and ψ_J , relations (5), in (3) such that:

$$\frac{k_b}{k_t} \propto \frac{EI}{GJ_T} = \frac{EI_D \psi_I}{GJ_D \psi_J} \quad (7)$$

Expressions of ψ_I , ψ_J and their ratio are given in Table 1a. For the class of proportionally scaled layers with double symmetry, ψ_I and ψ_J are constant regardless of their scaling and volume fraction, as shown in Table 1b.

For this work, 20 petiole specimens of the *Rheum rhabarbarum* were collected in Montreal (Canada) and analyzed. They are similar in shape and their geometric properties are reported in Table 2. The lower curved part roughly resembles a semielliptical profile, whereas the upper part is flat or grooved.

To formulate the shape transformers of the petiole cross-sections, we consider half of the symmetric shapes modeled in Table 1a, as illustrated in Table 3a. There, in addition to the families

Table 2: Geometry and shape transformers of specimen cross-sections.





















	Petiole cross-section	$\frac{B \text{ (mm)}}{H \text{ (mm)}}$	Area (mm ²)	ψ_A	$I \text{ (mm}^4\text{)}$	ψ_I	$J \text{ (mm}^4\text{)}$	ψ_J	λ_I	λ_J	$\frac{\psi_I}{\psi_J}$
1		39 25	681	0.70	23444	0.47	76841	0.44	0.67	0.63	1.05
2		28 13	242	0.67	2247	0.46	12354	0.44	0.68	0.65	1.05
3		29 15	309	0.71	4112	0.50	17496	0.45	0.71	0.64	1.11
4		35 23	551	0.67	16777	0.45	47899	0.40	0.67	0.59	1.13
5		25 16	303	0.76	4484	0.53	13417	0.46	0.69	0.60	1.15
6		23 18	297	0.74	4976	0.48	11614	0.41	0.66	0.56	1.17
7		32 21	469	0.71	11526	0.49	33338	0.42	0.70	0.59	1.18

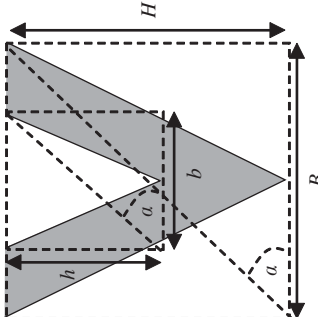
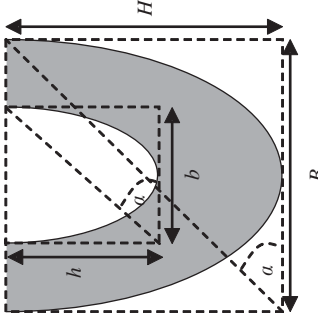
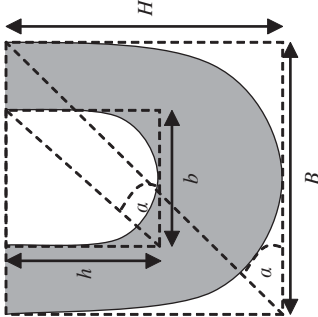
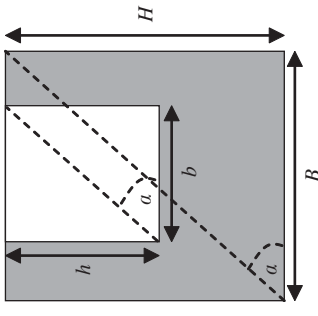
Table 2: (Continued)

	Petiole cross-section	$\frac{B \text{ (mm)}}{H \text{ (mm)}}$	Area (mm ²)	ψ_A	$I \text{ (mm}^4\text{)}$	ψ_I	$J \text{ (mm}^4\text{)}$	ψ_J	λ_I	λ_J	$\frac{\psi_I}{\psi_J}$
8		30 16	365	0.74	5860	0.53	21425	0.45	0.72	0.60	1.19
9		27 16	326	0.77	4923	0.58	16444	0.48	0.75	0.62	1.20
10		29 21	443	0.75	10687	0.51	26578	0.43	0.69	0.57	1.21
11		33 26	628	0.75	24205	0.53	52478	0.43	0.71	0.58	1.23
12		30 22	523.1	0.78	16122	0.57	34685	0.44	0.74	0.57	1.30
13		31 27	603	0.72	23680	0.47	41106	0.35	0.65	0.49	1.34
14		30 21	498	0.77	14161	0.58	31047	0.43	0.75	0.56	1.35
15		27 16	301	0.71	4628	0.53	13436	0.39	0.75	0.55	1.36
16		26 19	343	0.70	7216	0.51	15425	0.37	0.72	0.53	1.37
17		26 15	295	0.75	4403	0.59	12746	0.43	0.79	0.57	1.37
18		26 18	361	0.79	7143	0.60	16348	0.43	0.77	0.55	1.39
19		21 16	272	0.81	4551	0.63	8708	0.45	0.79	0.55	1.42
20		24 17	321	0.77	6483	0.62	11737	0.38	0.80	0.50	1.60

obtained with $n = 1$, $n = 2$, and $n \rightarrow \infty$, we chose $n = 2.5$ to match better the contours of the average petiole. Similar to Table 1b, Table 3b illustrates the ranges of the shape transformer ratios for bending resistance, torsional resistance and their ratio.

In the next section, the results are used to develop design maps that compare the petiole performance to that of common engineering cross-sections.

Table 3a: Shape transformers for semi-superelliptical concepts.

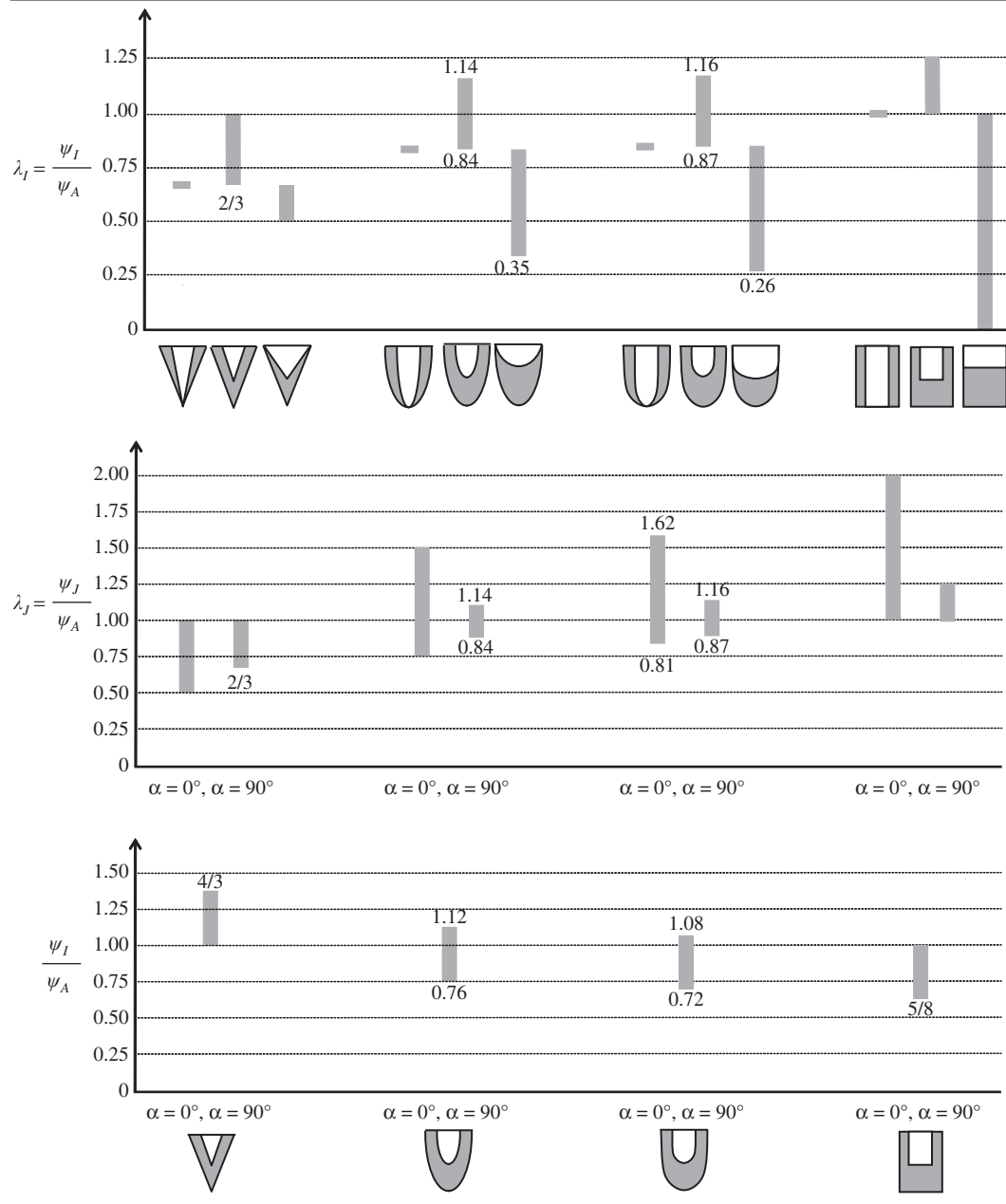
	$n = 1$	$\psi_A = \beta_1 [1 - cd]$		$n = 2$		$n = 2.5$		$n = \infty$
$\beta_1 = \frac{1}{2}$	$\psi_A = \beta_1 [1 - cd]$	$\beta_1 = \frac{\pi}{4}$	$\psi_A = \beta_1 [1 - cd]$	$\beta_1 = 0.85$	$\beta_1 = 1$			
$0 \leq \psi_A \leq \frac{1}{2}$		$0 \leq \psi_A \leq \frac{\pi}{4}$		$0 \leq \psi_A \leq 0.85$	$0 \leq \psi_A \leq 1$			
$\beta_2 = 1$	$\psi_I = \beta_2 [1 - cd^3 - PA]$	$\beta_2 = \frac{3\pi}{4}$	$\psi_I = \beta_2 [1 - cd^3 - PA]$	$\beta_2 = 2.74$	$\beta_2 = 4$			
$0 \leq \psi_I \leq \frac{1}{3}$		$0 \leq \psi_I \leq 0.69$		$0 \leq \psi_I \leq 0.74$	$0 \leq \psi_I \leq 1$			

$PA = \beta_3 \left[(cd^2 - 1)^2 (1 - cd)^{-1} \right]$			
$\beta_3 = \frac{2}{3}$	$\beta_3 = 0.72$	$\beta_3 = 0.73$	$\beta_3 = \frac{3}{4}$
$\lambda_I = \beta_4 \left[(1 - cd^3 - PA)(1 - cd)^{-1} \right]$			
$\beta_4 = 2$	$\beta_4 = 3$	$\beta_4 = 3.24$	$\beta_4 = 4$
$\frac{1}{2} \leq \lambda_I \leq 1$	$0.35 \leq \lambda_I \leq 1.14$	$0.26 \leq \lambda_I \leq 1.16$	$0 \leq \lambda_I \leq \frac{5}{4}$
$\psi_I = \beta_5 \left[1 - cd^3 + \cos^2 a \left(cd^3 - \frac{c^3 d}{4} - \frac{3}{4} \right) - \sin^2 a (PA) \right]$			
$\beta_5 = 1$	$\beta_5 = \frac{3\pi}{4}$	$\beta_5 = 2.74$	$\beta_5 = 4$
$a = 0^\circ : 0 \leq \psi_I \leq \frac{1}{4}$	$a = 0^\circ : 0 \leq \psi_I \leq 0.59$	$a = 0^\circ : 0 \leq \psi_I \leq 0.68$	$a = 0^\circ : 0 \leq \psi_I \leq 1$
$a = 90^\circ : 0 \leq \psi_I \leq \frac{1}{3}$	$a = 90^\circ : 0 \leq \psi_I \leq 0.66$	$a = 90^\circ : 0 \leq \psi_I \leq 0.74$	$a = 90^\circ : 0 \leq \psi_I \leq 1$

Table 3a: (Continued)

$\lambda_J = \beta_6 \left[\left(1 - cd^3 + \cos^2 a \left(cd^3 - \frac{c^3 d}{4} - \frac{3}{4} \right) - \sin^2 a (PA) \right) (1 - cd)^{-1} \right]$			
$\beta_6 = 2$	$\beta_6 = 3$	$\beta_6 = 3.23$	$\beta_6 = 4$
$a = 0^\circ : \frac{1}{2} \leq \lambda_J \leq 1$	$a = 0^\circ : \frac{3}{4} \leq \lambda_J \leq \frac{3}{2}$	$a = 0^\circ : 0.81 \leq \lambda_J \leq 1.62$	$a = 0^\circ : 1 \leq \lambda_J \leq 2$
$a = 90^\circ : \frac{2}{3} \leq \lambda_J \leq 1$	$a = 90^\circ : 0.84 \leq \lambda_J \leq 1.14$	$a = 90^\circ : 0.87 \leq \lambda_J \leq 1.16$	$a = 90^\circ : 1 \leq \lambda_J \leq \frac{5}{4}$
$\frac{\psi_I}{\psi_J} = \frac{1 - cd^3 - PA}{1 - cd^3 + \cos^2 a \left(cd^3 - \frac{c^3 d}{4} - \frac{3}{4} \right) - \sin^2 a (PA)}$			
$a = 0^\circ : 1 \leq \frac{\psi_I}{\psi_J} \leq \frac{4}{3}$	$a = 0^\circ : 0.76 \leq \frac{\psi_I}{\psi_J} \leq 1.12$	$a = 0^\circ : 0.72 \leq \frac{\psi_I}{\psi_J} \leq 1.08$	$a = 0^\circ : \frac{5}{8} \leq \frac{\psi_I}{\psi_J} \leq 1$
$a = 90^\circ : \frac{\psi_I}{\psi_J} = 1$	$a = 90^\circ : \frac{\psi_I}{\psi_J} = 1$	$a = 90^\circ : \frac{\psi_I}{\psi_J} = 1$	$a = 90^\circ : \frac{\psi_I}{\psi_J} = 1$

Table 3b: Range of shape transformers for semi-superelliptical concepts.



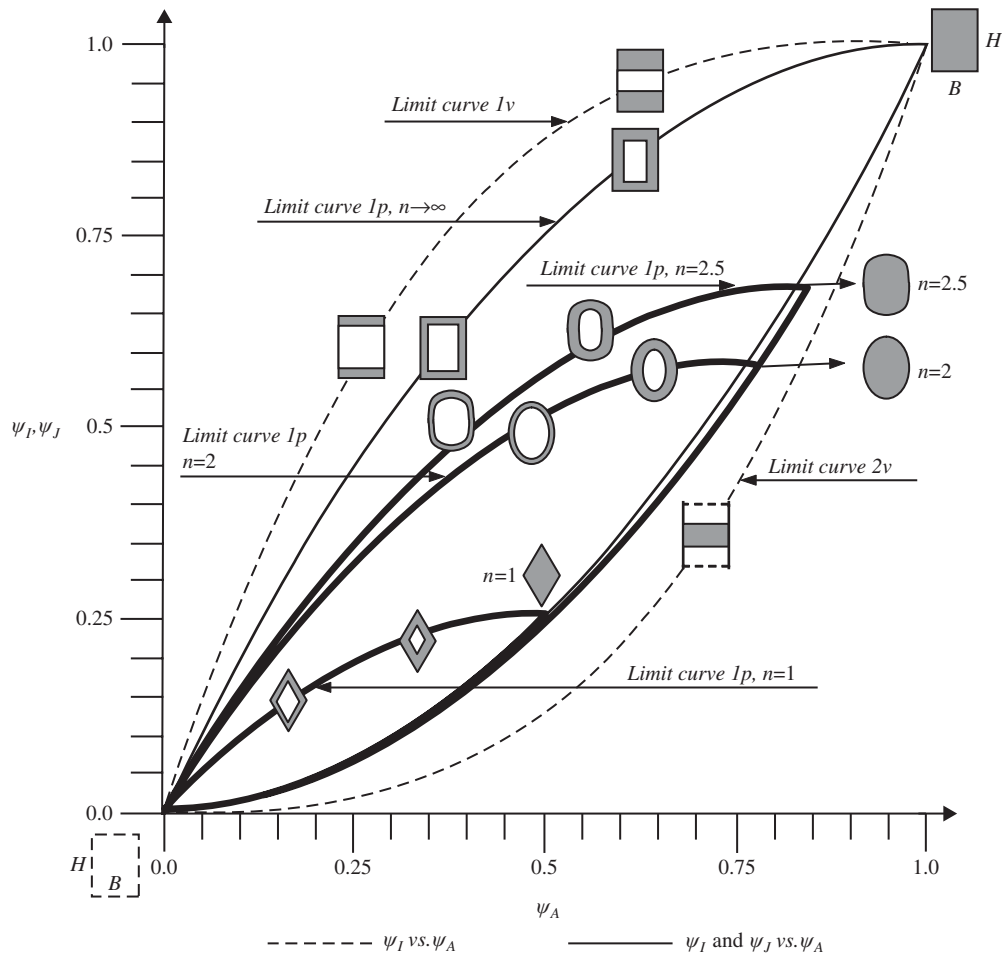


Figure 5: Flexural and torsional stiffness map for engineering cross-sections with double symmetry.

7 EFFICIENCY MAPS

Shape efficiency maps are presented here for pure bending stiffness, for torsion stiffness, and for the twist-to-bend ratio. As an example, the efficiency of symmetric engineering cross-sections (Table 1a and b) is illustrated in Section 7.1. Then, in Section 7.2., we map the properties of asymmetric shapes derived from half Lamé curves (Table 3a and b) and compare them with those of the petiole specimen (Table 2).

7.1 Engineering design maps

Figure 5 illustrates an example of a shape efficiency map. The flexural and torsional stiffness, ψ_I and ψ_{JT} , are plotted versus ψ_A using the expressions of Table 1a for shapes with symmetry along both horizontal and vertical directions. The continuous lines describe ψ_I and ψ_{JT} for hollow shapes where

the hole is proportionally scaled to the envelope. Hidden lines represent ψ_I for the vertically scaled layers class of the rectangle family.

The chart is based on the rationale explained in Section 6.1. The position of a cross-section is specified by the coordinates $[\psi_A = m/(\rho l A_D); \psi_g = F/(M G_D)]$ where in this case $\psi_g = \psi_I$, ψ_I and the parameters at the right hand side of ψ_A and ψ_g are constant for a given envelope. The slopes, λ_I and λ_J , from the origin to a point on the segments are the shape efficiency for bending and torsion stiffness respectively. Stiff and lightweight shapes, for example, lie on the top left of the chart.

When ψ_I is considered in Fig. 5, then the flexural stiffness of all cross-sectional shapes that partially fill the envelope, $B \times H$, falls in the region bounded by the limit curves 1v and 2v. These boundaries (i.e., dashed curves) characterize the class of the vertically scaled layers for the rectangles family, when the material fraction varies within an envelope of any size. Outside this area, no cross-sectional shape of the rectangles or any other family exists. The limit curve 1v represents idealized I cross-sections, whereas the limit curve 2v describes idealized H cross-sections. The former describes conditions where the material layer is vertically scaled and efficiently placed on the upper and lower surfaces of the cross-section. The latter refers to the scenario where the material layer is vertically scaled and placed closed to the neutral axis.

Whereas the dashed curves describe only bending stiffness, the continuous curves (i.e., curves 1p) characterize both the flexural and torsional stiffness for hollow cross-sections of the proportionally scaled layers class. The thin curves describe the rectangles ($n \rightarrow \infty$), the thicker ones represent the Lamé curve cross-sections for $n = 1$ (the diamonds), $n = 2$ (the ellipses), and $n = 2.5$ (the superellipses). As expected, the graph shows that for a given envelope, the higher the exponent n , the stiffer the cross-section (Table 1b). It is noted that whereas curves for the proportionally scaled layers of symmetric cross-section (continuous lines in Fig. 5) do not change with envelope scaling, those for other classes are dependent on the envelope size [24].

In the next section, such maps are used to contrast the performance of biological to ideal engineering shapes.

7.2 Nature design maps

In contrast to the cross-sections shown in Table 1a, the petiole shapes of the *Rheum rhabarbarum* specimen do not possess horizontal symmetry. For this reason, semi-super-elliptical shape have been modeled for $n = 1, 2, 2.5$, as shown in Table 3a. Their properties have been plotted in Figs 6–8 and compared with those of the petiole specimens (Table 2).

7.2.1 Flexural stiffness

Figure 6 illustrates the flexural stiffness of both symmetric (Table 1a) and asymmetric (Table 3a) superellipses with respect to fraction and location of material within the envelope. For pure bending stiffness, the curves ψ_I are invariant to any envelope scaling. This indicates that cross-section size changes have no impact on the flexural stiffness shape properties.

Figure 6 shows that asymmetric semi-superelliptical shapes are stiffer than the corresponding symmetric concepts for a given envelope and material volume. For example, the hollow shapes with double symmetry obtained for $n = 2$ and $n = 2.5$ are stiffer than their respective half-Lamé curves concepts for $\psi_A < (\psi_A)_C$ and $\psi_A < (\psi_A)_D$. But for $\psi_A > (\psi_A)_C$ and $\psi_A > (\psi_A)_D$, the half-Lamé curves make a more economical use of material when they are almost solid. The diamonds ($n = 1$), however, can never be as stiff as the triangle ($n = 1$) for any value of ψ_A . Here, the stiffness gain (FG) is maximum for $\psi_A = 0.5$ (i.e., when the shapes are solid).

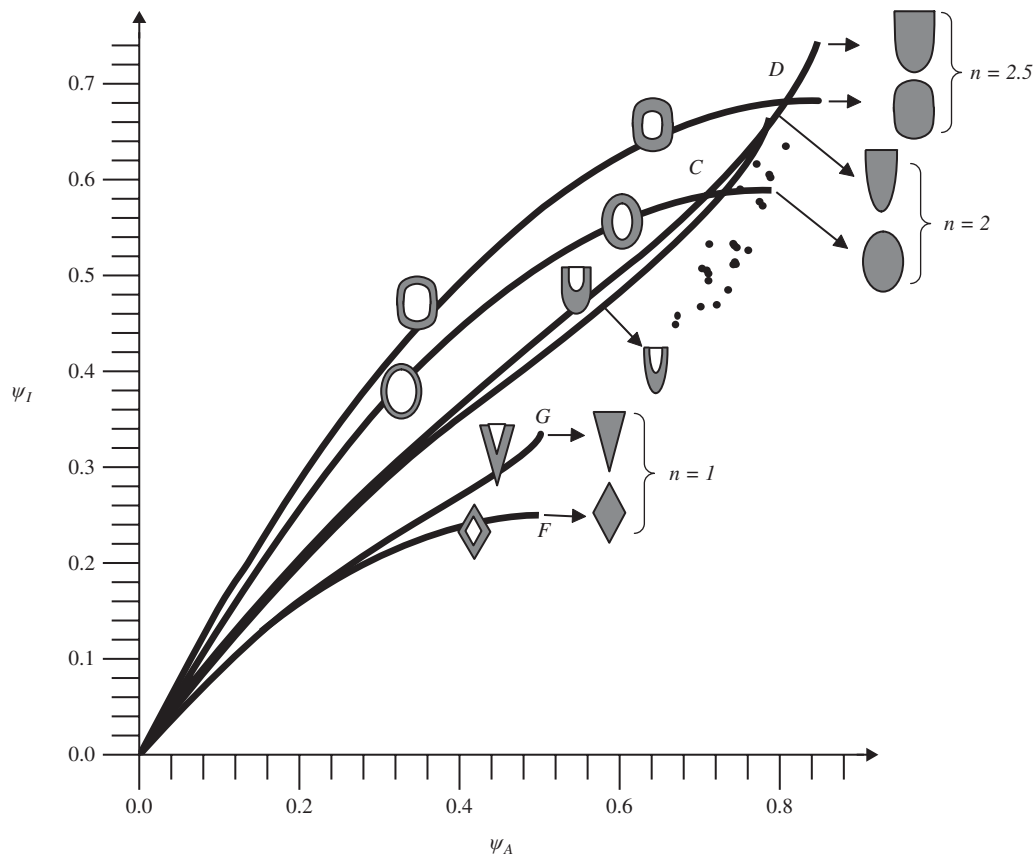


Figure 6: Flexural stiffness curves for cross-sections with vertical axis symmetry and flexural stiffness coordinates for petiole specimens (Table 2).

Table 2 shows that λ_I ranges from 0.65 to 0.79 for petiole specimens. Their shapes are almost solid with a top profile that is slightly grooved or flattened with rounded corners. Compared to hollow ideal cross-sections, the solid shapes of the petiole perform relatively well, as shown by the plot of their properties in Fig. 6.

7.2.2 Torsional stiffness

Unlike ψ_p , ψ_J for asymmetric shapes depends on the ratio of the envelope size. The plot of ψ_J vs. ψ_A (Table 3a) in Fig. 6 shows that heightwise scaling makes asymmetric shapes stiffer in torsion. The deeper the envelopes, the stiffer the half-superellipses. For example, the semi-ellipses class stretched widthwise to the limit $a \rightarrow 0$ and the ellipses regardless of a are equally stiff and described by the same curves. But if the former is scaled heightwise with $a > 0$, then their torsional stiffness increases and shifts upward until the upper bound (i.e., curve asy, $a \rightarrow 90$). This effect does not occur for double symmetric shapes of the proportionally scaled layers class.

The shaded regions describe the effect of scaling on the shape properties for torsional stiffness. Within them, lies the torsional stiffness of each asymmetric shape concept for any envelope scaling

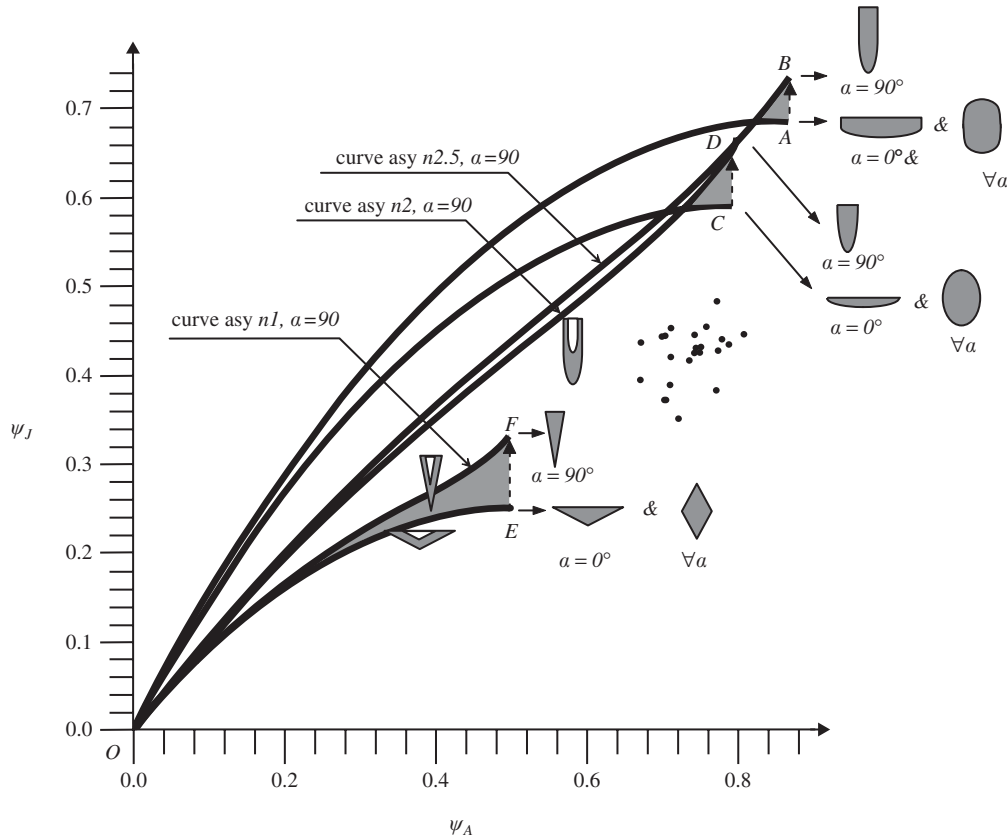


Figure 7: Torsional stiffness described by curves for cross-sections with vertical symmetry and by points for petiole specimens (Table 2).

$0 < a < 90$. Thus, widthwise stretching increases torsional compliance until the low bound ($a \rightarrow 0$) of each concept.

Plotting the shape transformers of the specimens in Fig. 6 (Table 2) allows gaining an insight into the torsional compliancy of the petiole cross-section shape. The petiole cross-sections are asymmetric and stretched widthwise. Their efficiency in torsion resistance is very low. Their range of λ_J between 0.49 and 0.64 (Table 3b) shows that the petiole design can ease the leave sway in wind.

7.2.3 Flexural vs. torsional stiffness

The aim of this section is to develop a map of ψ_I versus ψ_J to gain insight into the shape properties that make a cross-section more capable to twist than bend under given forces.

In Fig. 8, expressions given in Tables 1a and 2a are used to illustrate the relation $\psi_I = f(\psi_J)$. On this map, the index ψ_I/ψ_J is the slope of the line between the origin and a point on the curve. For a given envelope, the steeper the slope, the easier it is to twist the shape. In the shaded region above the quadrant bisector, there are shapes that twist before bending and thus have ψ_I/ψ_J greater than one. Below, lie shapes that are more flexible under bending load.

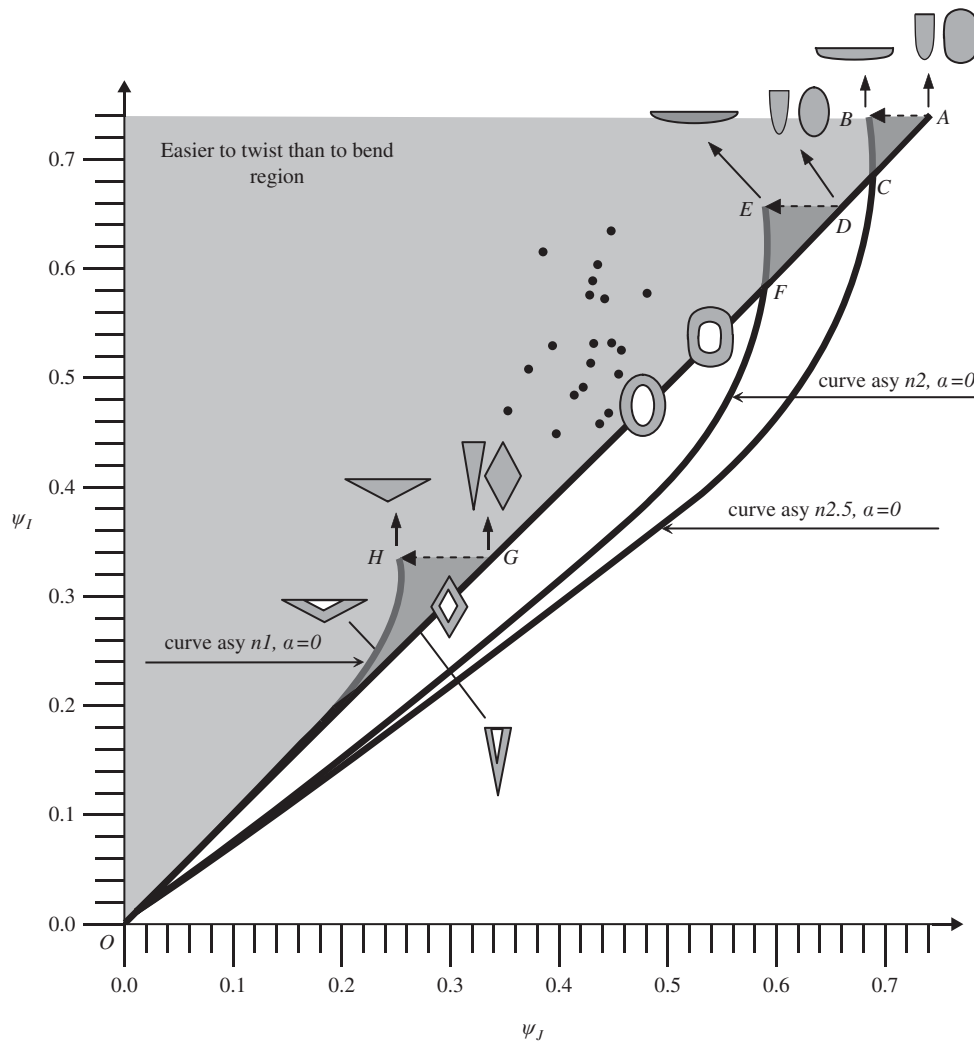


Figure 8: Twist-to-bend ratio curves and points for cross-sections with vertical symmetry and for petiole specimens respectively.

The bisector describes different shape concepts that are equally rigid in torsion and bending. The bisector represents not only the three shape families with double symmetry obtained for $n = 1, 2, 2.5$ (Table 1b) for proportionally scaled layers, but also the corresponding asymmetric shape concepts. These are half superellipses for the ideal case where the cross-section width is stretched to its limit ($a \rightarrow 90$).

For a prescribed ψ_I , it is possible to lower the torsional stiffness without losing resistance to bending. This effect is shown in Fig. 8 by scaling the semi-super-ellipses. If scaling is applied to a solid shape with $a \rightarrow 90$ (e.g., points A, D, G) (Fig. 8), then flattening the cross-section widthwise until $a \rightarrow 0$ (e.g., B, E, H) increases the twist-to-bend ratio. For $0 < a < 90$, the shape properties will fall respectively between A and B, D and E, G and H.

Among the semi-superellipses with prescribed envelopes, the triangle has the best potential to maximize ψ_I/ψ_J , as shown by the ranges indicated in Table 3b. This trend is also evident in Fig. 8 by comparing the shaded areas ABC, DEF and GHO. The size of these regions decreases with the increase of the power, n , of the Lamé curves. This shows that widthwise stretching is always beneficial to maximize ψ_I/ψ_J for solid and hollow triangles. On the contrary, stretching superellipses with $n = 2.5$ and $n = 2$ widthwise is beneficial only when $\psi_J > (\psi_J)_C$ and $\psi_J > (\psi_J)_F$ (i.e., when the cross-section is almost solid).

Table 2 reports the twist-to-bend ratio of the petiole specimens ranked in ascending order in terms of ψ_I/ψ_J . For all specimens, $\psi_I/\psi_J > 1$ and their range is between 1.05 and 1.60. Such cross-sections are stretched widthwise, their heights are smaller than widths, and they have asymmetric shapes with a grooved or flat top that resemble superellipses with $n = 2.5$. The plot of their shape transformers in Fig. 8 shows that the specimens have high ψ_I/ψ_J that lower the torsional stiffness of the structure without compromising their deflection resistance to gravity loading. This flexibility allows the leaves to bunch, orient themselves towards downwind, and reduce wind drag.

As described in previous sections, the structural performance of the petiole is governed by material and geometry. In this preliminary analysis, the former has been considered uniform and the latter has been modeled only at the meso-scale. The maps presented here help to gain insight into geometric features, such as cross-section shapes, symmetry, and scaling. A similar approach can be applied to model the microstructure at the tissue level and to develop maps that illustrate how Nature tailors Young's modulus and Shear modulus at the micro-scale. This will be the focus of future investigations.

The study of biological structures is crucial to the development of novel biomimetic technology. Unlocking the mechanisms used by plants to grow their flexible and resistant structures is a pathway to discover new advanced engineering materials. Current engineering technology fails to fully exploit the structural and functional integration found in plants at each length scale, from cell formation to tissue specialization. Further progress in bio-inspired material design requires biology, engineering modeling and structural optimization with the ultimate goal of developing compliant materials and structures based on natural principles of self-assembly, anisotropic growth, cell division, and shape optimization.

8 CONCLUSIONS

This paper has examined the shape performance of the leaf petiole of *Rheum rhabarbarum* plants. The twist-to-bend ratio has been used to assess the efficiency of the cross-section shape in minimizing wind drag as well as in preventing the sag under gravity loads. The shape properties of 20 specimens have been contrasted to those of ideal engineering cross-sections. To best fit the petiole specimen, the ideal shapes have been chosen with double and single axes symmetry and with different superellipse profiles.

Efficiency maps have been developed to gain a visual insight into shape and size efficiency of cross-sections. The charts have shown that the characteristic grooved non-circular flattened cross-section eases the twist of the petiole without lowering its flexural stiffness. On the contrary, circular and elliptical shapes, which are commonly found in other plant organs (e.g., the stem), offer an equal resistance to bending and torsion, and thus are not the best to meet the structural requirements of the petioles.

The modeling approach and the efficiency maps developed in this paper can be extended to examine the material microstructure and illustrate the impact that material anisotropy has on the twist-to-bend ratio. This work is a first step to the development of biomimetic compliant materials and structures.

ACKNOWLEDGMENTS

The author thanks Mr. Andrew Laughton and Mr. Adenariwo Adepoju, third year undergraduates of Mechanical Engineering at McGill University, for their generous help in finalizing the tables and pictures.

NOMENCLATURE

A	cross sectional area (m^2)
B	width (m)
b	internal width (m)
D	cross-section envelope dimensions (b, h)
E	Young's modulus (GPa)
F	functional requirements
g	geometric quantity, such as the second moment of area
G	Shear Modulus (GPa)
h	internal height (m)
H	height (m)
I_{xx}	second moment of area about cross-section horizontal axis (m^4)
k_b, k_t	linear (N/m) and torsional (N m/rad) stiffness requirement
J_T	Torsional constant (m^4)
λ_p, λ_j	shape lightweight efficiency parameters for bending and torsion stiffness design
L	length (m)
m	mass (mg)
M	bending moment (N m)
n	integer of Lamé curves
S	shape of the cross-section
T	twisting moment (N m)
ρ	material density (mg/m^3)
ψ_g	shape transformer of a given geometric quantity g

REFERENCES

- [1] Campbell, N.A., Reece, J.B. & Mitchell, L.G., *Biology*, 5th edn, Benjamin Cummings: Don Mills, 1999.
- [2] Wainwright, S.A., Biggs, W.D., Currey, J.D. & Gosline, J.M., *Mechanical Design in Organisms*, Princeton University Press, 1982.
- [3] Vogel, S., Drag and reconfiguration of broad leaves in high winds. *Journal of Experimental Botany*, **40**, pp. 941–948, 1989.
- [4] Niklas, K.J., The mechanical roles of clasping leaf sheaths: evidence from *Arundinaria tecta* shoots subjected to bending and twisting forces. *Annals of Botany*, **81**, pp. 23–34, 1998.
- [5] Etnier, S.A. & Vogel, S., Reorientation of daffodil followers in wind: drag reduction and torsional flexibility. *American Journal of Botany*, **87**, pp. 29–32, 2000.
- [6] Vogel, S., Twist-to-bend ratio ratios of woody structures. *Journal of Experimental Botany*, **46**, pp. 981–985, 1995.
- [7] Vogel, S., Drag and flexibility in sessile organisms. *Am. Zool.*, **24**, pp. 37–44, 1984.
- [8] Vogel, S., *Comparative Biomechanics: Life's Physical World*, Princeton University Press, 2003.
- [9] Koehl, M.A.R., Effects of sea anemones on the flow forces they encounter. *Journal of Experimental Botany*, **69**, pp. 87–105, 1977.

- [10] Koehl, M.A.R., Mechanical organization of cantilever-like sessile organisms: sea anemones. *Journal of Experimental Botany*, **69**, pp. 127–142, 1977.
- [11] Ennos, A.R., The mechanics of the flower stem of the sedge *Carex acutiformis*. *Annals of Botany*, **72**(2), pp. 123–127, 1993.
- [12] Ennos, A.R., Spatz, H.C. & Speck, T., The functional morphology of the petioles of the banana, *Musa textilis*. *Journal of Experimental Botany*, **51**(353), pp. 2085–93, 2000.
- [13] Etnier, S.A., Flexural and torsional stiffness in multi-jointed biological beams. *Biological Bulletin*, **200**(1), pp. 1–8, 2001.
- [14] Etnier, S.A., Twisting and bending of biological beams: distribution of biological beams in a stiffness mechanospace. *Biological Bulletin*, **205**(1), pp. 36–46, 2003.
- [15] Vogel, S., Twist-to-bend ratios of woody structures. *Journal of Experimental Botany*, **46**, pp. 981–985, 1995.
- [16] Niklas, K.J., The elastic moduli and mechanics of *Populus tremuloides* (Salicaceae) petioles in bending and torsion. *American Journal of Botany*, **78**, pp. 989–996, 1991.
- [17] Harder, D.L., Hurd, C.L. & Speck, T., Comparison of mechanical properties of four large, wave-exposed seaweeds. *American Journal of Botany*, **93**(10), pp. 1426–1432, 2006.
- [18] Gallenmüller, F., Müller, U., Rowe, N.P. & Speck, T., The growth form of *Croton pullei* (Euphorbiaceae) – functional morphology and biomechanics of a neotropical liana. *Plant Biol.*, **3**, pp. 50–61, 2001.
- [19] Niklas, K.J., *Plant Biomechanics: An Engineering Approach to Plant Form and Function*, University of Chicago Press: Chicago, IL, 1992.
- [20] Pasini, D. & Mirjalili, V., The optimized shape of a leaf petiole. *3rd International Conference on Design and Nature*, Wessex, UK, pp. 35–45, May 24–26, 2006.
- [21] Pasini, D., Shape Transformers for Material and Shape Selection of Lightweight Beams, *Journal of Materials and Design*, Vol. **28**(7), pp. 2071–2079, 2007.
- [22] Pasini, D., Material and shape selection for optimizing flexural vibrations in multilayered resonators. *Journal of Microelectromechanical Systems*, **15**(6), pp. 1745–1758, 2006.
- [23] Pasini, D., Burgess, S.C. & Smith, D.J., A method for selecting macro-scale structures with axially loaded members. *International Journal of Mechanics and Materials in Design*, **3**, pp. 185–199, 2006.
- [24] Mirjalili, V. & Pasini, D., Shape efficiency maps for optimum shape selection in torsion stiffness design. *18th IASTED International Conference on Modelling and Simulation*, May 30–June 1, Montreal, 2007.
- [25] Loria, G., *Spezielle algebraische und transscendente ebene kurven: Theorie and Geshichte*, B.G. Teubner: Leipzig, 1902.
- [26] Gardner, M., The superellipse: a curve that lies between the ellipse and the rectangle. *Scientific American*, **213**, pp. 222–234, 1965.
- [27] Gridgeman, N.T., Lamé ovals. *Mathematical Gazette*, **54**, p. 31, 1970.
- [28] Gibson, C.G., *Elementary Geometry of Algebraic Curves*, Cambridge University Press, Cambridge, 1998.
- [29] Jaklic, A., Leonardis, A. & Solina, F., *Segmentation and Recovery of Superquadrics*, Kluwer Academics Publishers: Dordrecht, Boston, London, 2000.
- [30] Thomson, D'A.W., *On Growth and Form*, Cambridge University, Press: Cambridge, UK, 1917.
- [31] Gielis, J., A generic geometric transformation that unifies a wide range of natural and abstract shapes. *American Journal of Botany*, **90**, pp. 333–338, 2003.
- [32] Gielis, J., Superquadrics with rational and irrational symmetry. *SM'03*, June 16–20, pp. 16–20, Seattle, Washington, USA, 2003.

- [33] Peterson, I., A geometric superformula. *Science News*, **163(18)**, 2003.
- [34] Meyers, M.A., Lin, A.Y.M., Seki, Y., Chen, P.-Y., Kad, B.K. & Bodde S., Structural biological composites: an overview, *JOM*, **58(7)**, pp. 35–41, 2006.
- [35] Burgess, S.C., Multifunctioning and multi-optimisation in feathers. *International Journal of Design and Nature*, **1**, pp. 1–10, 2007.
- [36] McMahon, T.A., Size and shape in biology. *Science*, **179**, pp. 1201–1204, 1973.
- [37] Mattheck, C., Engineering components grow like trees. *Kernforschungszentrum Karlsruhe*, **67**, pp. 1661–1686, 1989.
- [38] Mattheck, C., *Trees: The Mechanical Design*, Springer-Verlag: Berlin, 1991.
- [39] Gere, J.M. & Timoshenko, S.P., *Mechanics of Materials*, Brooks/Cole Engineering Division: Monterey, CA, 1984.
- [40] Boresi, A.P. & Schmidt, R.J., *Advanced Mechanics of Materials*, John Wiley & Sons: New York, 2003.
- [41] Sidenbladh, G., Stockholm: a planned city. *Cities: Their Origin, Growth and Human Impact*, WH Freeman: San Francisco, 1973.